Journal of Experimental and Theoretical Physics, Vol. 90, No. 6, 2000, pp. 1081–1088.
Translated from Zhurnal Éksperimental'noĭ i Teoreticheskoĭ Fiziki, Vol. 117, No. 6, 2000, pp. 1242–1250.

SOLIDS
Electronic Properties

Influence of Silver on the Galvanomagnetic Properties and Energy Spectrum of Mixed $(Bi_{1-x}Sb_x)_2Te_3$ Crystals

V. A. Kul'bachinskiĭ[a, *], A. Yu. Kaminskiĭ[a], V. G. Kytin[a], P. Lošťak[b], Č. Drašar[b], and A. de Visser[c]

Moscow State University, Moscow, 119899 Russia
**e-mail: kulb@mig.phys.msu.su*
[b]*Pardubice University, Pardubice, Czech Republic*
[c]*Van der Waals Institute, University of Amsterdam, the Netherlands*

Received January 25, 2000

Abstract—An investigation is made of the temperature dependences of the resistivity in the range 4.2–300 K, the Hall effect, and the Shubnikov–de Haas effect in magnetic fields up to 40 T in $(Bi_{1-x}Sb_x)_2Te_3Ag_y$ single crystals ($0 \le x \le 0.75$). Doping $(Bi_{1-x}Sb_x)_2Te_3$ crystals with silver showed that in Sb_2Te_3 and $(Bi_{1-x}Sb_x)_2Te_3$ crystals unlike Bi_2Te_3 silver exhibits acceptor properties. The angular and concentration dependences of the Shubnikov–de Haas effect were studied in $(Bi_{1-x}Sb_x)_2Te_3Ag_y$. It was established that the anisotropy of the ellipsoids of the upper valence band in $Bi_{0.5}Sb_{1.5}Te_3$ remains unchanged as a result of silver doping. © *2000 MAIK "Nauka/Interperiodica".*

1. INTRODUCTION

Semiconductors of the Sb_2Te_3 type are layered crystals having a rhombohedral structure and symmetry space group R_{3m}–D_{3d}^5 with the twofold and threefold axes of symmetry C_2 and C_3. The crystal lattice is formed by periodically ordered layers lying in the plane perpendicular to the C_3 symmetry axis. Each layer consists of five atomic planes (quintets) forming the following sequence: Te^1–Sb–Te^2–Sb–Te^1. Here Te^1 and Te^2 denote Te atoms in various positions. In each individual layer the atoms are similar and form a plane hexagonal lattice. The atoms of each successive layer are positioned above the centers of the triangles formed by atoms of the preceding layer (hexagonal close packing), i.e., the Te^1 and Sb atoms occupy octahedral positions in a tetradymite structure. The chemical bond within the quintets is covalent-ionic. Between the quintets there is a comparatively large spacing and a weak bond produced by van der Waals forces. This is responsible for the anisotropy of the electrophysical properties of single crystals [1].

Crystals of Sb_2Te_3 have a very high concentration of holes because of the presence of a large number of charged point defects. Single crystals of Sb_2Te_3 typically have the following types of defects: Sb and Te vacancies, atoms of these elements in interstitial sites, antistructural Sb_{Te} (an Sb atom in a Te position) and Te_{Sb} defects (a Te atom in an Sb position), impurity antistructural defects, impurity atoms in interstitial sites, and so on. Since antistructural defects are negatively charged, Sb_2Te_3 grown under stoichiometric conditions always possesses *p*-type conductivity and has a fairly high hole concentration. Similar defects may be found in antimony telluride solid solutions.

Antistructural defects in Sb_2Te_3 semiconductors are formed under the influence of the bond polarity. The weak polarity of the Sb–Te bonds is conducive to the formation of antistructural defects. A change in the polarity of the bonds caused by doping or a shift of the stoichiometry leads to a change in the concentration of antistructural defects (see, for example, [2, 3]). Assuming that the charge of the antistructural defects is compensated by holes, any change in the concentration of antistructural defects will correspond to a change in the hole concentration. Dopants in layered crystals such as antimony telluride have a strong influence on the concentration of point defects and therefore on the carrier concentration. Consequently doping with elements in particular groups of the periodic table may have a donor or acceptor effect not depending on the number of the group but as a result of the influence of the incorporated element on the bond polarity. As an example we can quote the Group III element indium which has a donor effect in Sb_2Te_3 [4].

Mixed crystals, i.e., crystals of the type $(Bi_{1-x}Sb_x)_2Te_3$ or $Sb_2Te_{3-y}Se_y$ are of particular interest because the highest thermoefficiencies *Z* are observed in these. Different combinations of the elements Bi, Sb, As and Te, Se, S are possible. Despite intensive studies, very little data are currently available on the influence of doping with Group I elements on the energy spectrum of mixed $(Bi_{1-x}Sb_x)_2Te_3$ crystals.

1063-7761/00/9006-1081$20.00

Table 1

Samples	y determined by AAS	c, 10^{19} atoms/cm^3
$Sb_2Te_3Ag_y$	0.0035	2.2
	0.0093	5.9
	0.0100	6.2
	0.0152	9.6
$Bi_{0.5}Sb_{1.5}Te_3Ag_y$	0.0014	0.8
	0.0030	1.9
	0.0048	3.0

The Shubnikov–de Haas effect is an effective method of studying semiconductors since the parameters of the energy spectrum can be determined directly, i.e., the effective masses, Fermi surface cross sections, carrier concentration, and so on. However, in antimony telluride and mixed crystals such measurements are difficult since quantum oscillations of the magnetoresistance are initiated in magnetic fields having an induction higher than 10 T because of the fairly low hole mobility.

In the present study we investigated the Shubnikov–de Haas effect in magnetic fields up to 40 T which allowed us to observe oscillations of the magnetoresistance in all the samples studied. We also studied the influence of silver doping on the galvanomagnetic properties and energy spectrum of mixed $(Bi_{1-x}Sb_x)_2Te_3$ single crystals.

2. SAMPLES AND METHOD OF MEASUREMENT

We investigated *p*-type single-crystal samples of silver-doped antimony telluride Sb_2Te_3 and mixed $(Bi_{1-x}Sb_x)_2Te_3$ crystals grown by the Bridgman method from polycrystalline materials. First we synthesized polycrystalline samples from 99.999% pure elements in stoichiometric ratio in a quartz ampoule. We then added silver to the stoichiometric polycrystal for doping so that the sample compositions will subsequently be given in the form $Sb_2Te_3Ag_y$ and $(Bi_{1-x}Sb_x)_2Te_3Ag_y$. After preparing a polycrystal of the required composition we grew the single crystals. The grown single crystals were released from the quartz ampoule and cleaved perpendicular to the C_3 axis which, in the as-grown ingots, was always perpendicular to the longitudinal axis of the sample. The samples for the measurements, in the form of a parallelepiped having average dimensions of $1 \times 1 \times 5$ mm^3 with the long axis directed along the C_2 axis, were cut using an electric-arc machine. Current and potential leads made of 30 μm diameter copper wire were soldered using Bi + 4%Sb alloy.

The Ag content in the samples was determined by atomic absorption spectroscopy (AAS) for the specific sample used for all the electrophysical measurements. Table 1 gives the silver content y determined by AAS for the investigated samples and the experimentally determined silver concentration c in the measured samples. Attempts to obtain single crystals having an even higher silver content resulted in its segregation.

The Hall effect was investigated at temperatures of 4.2 K, 77 K, and 300 K. The dc current was directed along the C_2 axis and the magnetic field induction vector **B** was directed along the C_3 axis. The magnetic field at 4.2 K was generated by two methods. For measurements in fields not exceeding 11 T it was generated using a superconducting solenoid immersed in liquid helium. The measurements were made for two directions of the magnetic field induction vector and the Hall voltage was taken as half the difference between these values. In addition, the samples selected for the measurements had symmetrically positioned Hall contacts, i.e. in the absence of a magnetic field the potential from the Hall contacts was zero. For measurements in strong magnetic fields up to 40 T we used a pulsed magnetic field. In one of the $Bi_{0.5}Sb_{1.5}Te_3Ag_{0.003}$ samples the oscillations of the magnetoresistance were investigated by rotating the magnetic field in the C_3C_1 plane (see below).

3. RESULTS OF MEASUREMENTS

3.1. Galvanomagnetic Properties of $(Bi_{1-x}Sb_x)_2Te_3Ag_y$

Tables 2 and 3 give the resistivity ρ, Hall coefficients R, and Hall mobility μ of $(Bi_{1-x}Sb_x)_2Te_3Ag_y$ crystals at various temperatures. It should be noted that R does not depend on the magnetic field for all samples. Figure 1 gives the dependences $\rho(T)$ for various samples. For all samples the value of ρ decreases with decreasing temperature and saturates at low temperatures. In the temperature range 77–300 K the resistivity depends on temperature as $\rho \propto T^m$ where $m \approx 1.1$ for $Sb_2Te_3Ag_y$ and for $Bi_{0.5}Sb_{1.5}Te_3Ag_y$ samples. The small difference between this value of m and that of $m = 1.5$ typical of acoustic phonon scattering may be attributed to the additional scattering on ionized impurities and a possible temperature dependence of the effective mass when the current is directed along the C_2 axis. For a magnetic field parallel to the C_3 axis direct measurements have established that the cyclotron mass does not depend on temperature [5].

The Hall coefficients R are positive for all samples and depend on temperature: as the temperature decreases from room temperature to liquid-nitrogen temperature, the value of R decreases slightly and then remains almost constant (see Table 2 for $Sb_2Te_3Ag_y$ and Table 3 for $Bi_{0.5}Sb_{1.5}Te_3Ag_y$. This $R(T)$ dependence is typical of Sb_2Te_3 single crystals and may be explained quantitatively by the existence of two groups of holes belonging to the upper and lower valence bands, having different masses and probabilities (see, for example [6]). In the silver-doped samples R decreases monotonically with increasing Ag content, which indicates an

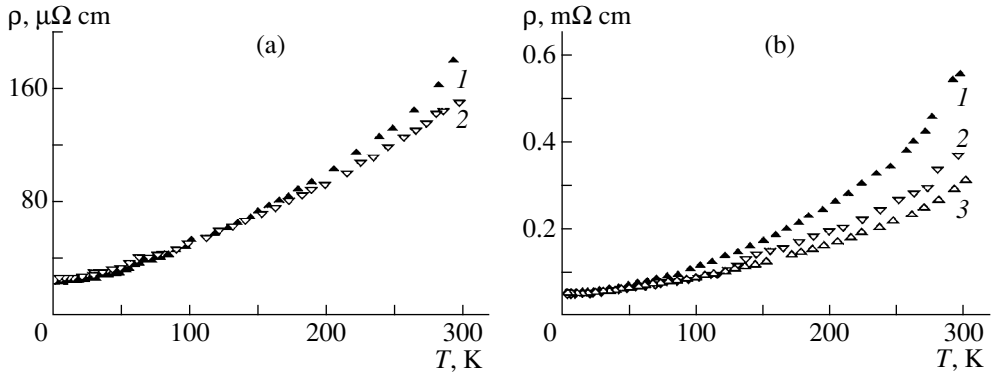

Fig. 1. Temperature dependences of the resistivity $\rho(T)$ for various $Sb_2Te_3Ag_y$ samples (a): (*1*) $Sb_2Te_3Ag_{0.0035}$; (*2*) $Sb_2Te_3Ag_{0.015}$ and $(Bi_{1-x}Sb_x)_2Te_3Ag_y$ (b): (*1*) $(Bi_{1-x}Sb_x)_2Te_3$, (*2*) $(Bi_{1-x}Sb_x)_2Te_3Ag_{0.0014}$, (*3*) $(Bi_{1-x}Sb_x)_2Te_3Ag_{0.0030}$.

increase in the hole concentration. The Hall coefficients do not depend on the magnetic field for all samples. The Hall mobility μ in the silver-doped samples decreases with increasing silver content at all temperatures, the decrease in μ being greater for $(Bi_{0.25}Sb_{0.75})_2Te_3Ag_y$ than for $Sb_2Te_3Ag_y$, as is illustrated in Fig. 2.

It can be seen from the doping results that the average efficiency of silver in $(Bi_{0.25}Sb_{0.75})_2Te_3$ crystals is lower than that in Sb_2Te_3 crystals, i.e., the number of additional holes per silver atom is lower in $(Bi_{0.25}Sb_{0.75})_2Te_3$. This result may be explained by the fact that in Sb_2Te_3 silver mainly enters the Sb sublattice and forms negatively charged substitutional point defects whereas in Bi_2Te_3 silver forms interstitial atoms. This is because the Bi–Te atomic bonds in Bi_2Te_3 crystals are more ionic than the Sb–Te bonds in Sb_2Te_3 crystals. The negative charge of the Te^1 and Te^2 atoms in the Bi_2Te_3 lattice is approximately an order of magnitude higher than the negative charge of the same atoms in the Sb_2Te_3 lattice. Similarly the positive charge of the Bi atoms in Bi_2Te_3 is an order of magnitude higher than the positive charge of Sb in Sb_2Te_3. Thus, very few point defects where Bi is substituted by Ag are formed in the Bi_2Te_3 lattice. At the same time, the incorporation of Ag suppresses the formation of antistructural negatively charged Bi_{Te}

Table 2. $Sb_2Te_3Ag_y$

y	$\rho^{4.2}$, mΩ cm	ρ^{77}, mΩ cm	ρ^{300}, mΩ cm	$R^{4.2}$, cm³/C	R^{77}, cm³/C	R^{300}, cm³/C	$\mu_H^{4.2}$, m²/V s	μ_H^{77}, m²/V s	μ_H^{300}, m²/V s
0	0.031	–	0.250	0.059	–	0.086	0.190	–	0.034
0.0035	0.023	0.050	0.180	0.028	0.020	0.035	0.122	0.040	0.019
0.0093	0.021	0.044	0.149	0.022	0.021	0.030	0.105	0.048	0.020
0.010	0.027	0.042	0.146	0.012	0.016	0.020	0.044	0.038	0.014
0.015	0.026	0.038	0.145	0.009	0.012	0.013	0.035	0.031	0.009

Table 3. $Bi_{0.5}Sb_{1.5}Te_3Ag_y$

y	$\rho^{4.2}$, mΩ cm	ρ^{77}, mΩ cm	ρ^{300}, mΩ cm	$R^{4.2}$, cm³/C	R^{77}, cm³/C	R^{300}, cm³/C	$\mu_H^{4.2}$, m²/V s	μ_H^{77}, m²/V s	μ_H^{300}, m²/V s
0	0.052	0.092	0.557	0.091	0.078	0.110	0.175	0.085	0.020
0.0014	0.047	0.077	0.366	0.037	0.030	0.050	0.079	0.039	0.014
0.0030	0.049	0.078	0.309	0.031	0.028	0.046	0.063	0.036	0.015
0.0048	0.044	0.073	0.333	0.016	0.025	0.044	0.036	0.034	0.013

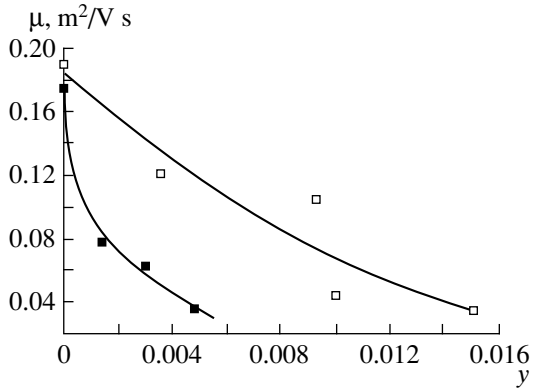

Fig. 2. Dependences of the Hall mobility μ at $T = 4.2$ K on the silver content y in $Sb_2Te_3Ag_y$ (open squares) and $(Bi_{1-x}Sb_x)_2Te_3Ag_y$ (filled squares).

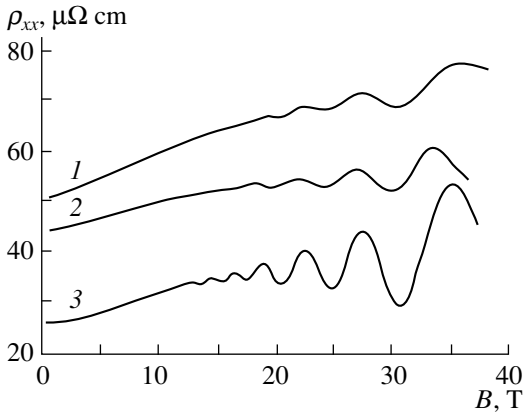

Fig. 3. Oscillations of the transverse magnetoresistivity ρ_{xx} of $Sb_2Te_3Ag_y$ samples at $T = 4.2$ K for samples having y contents: (*1*) 0.0093; (*2*) 0.010; (*3*) 0.015. Curves *1* and *2* are shifted upward.

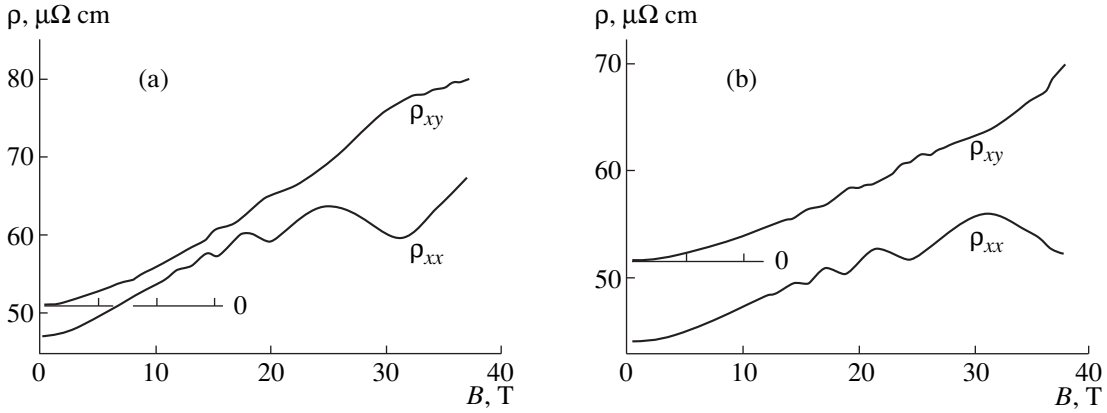

Fig. 4. Oscillations of the transverse magnetoresistivity ρ_{xx} and the Hall resistivity ρ_{xy} for (a) $Bi_{0.5}Sb_{1.5}Te_3Ag_{0.0014}$ and (b) $Bi_{0.5}Sb_{1.5}Te_3Ag_{0.0048}$ samples at $T = 4.2$ K. The dependences $\rho_{xy}(B)$ are measured from zero.

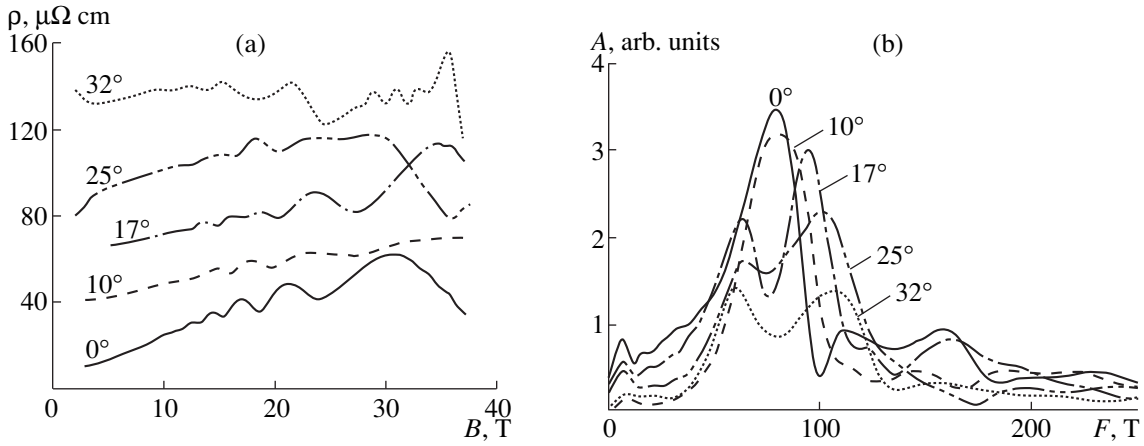

Fig. 5. Angular dependences of oscillations of the transverse magnetoresistivity ρ_{xx} in a $Bi_{0.5}Sb_{1.5}Te_3Ag_{0.0003}$ crystal and their Fourier spectra.

defects. All this gives rise to a different type of defect and ultimately to different behavior of Ag: in Sb_2Te_3 silver behaves as an acceptor whereas in Bi_2Te_3 silver doping induces a donor effect [7]. It is then easy to understand why the efficiency of silver as an acceptor is lower in a mixed $(Bi_{0.25}Sb_{0.75})_2Te_3Ag_y$ crystal.

3.2. Shubnikov–de Haas Effect in $(Bi_{1-x}Sb_x)_2Te_3Ag_y$ Crystals

Shubnikov–de Haas oscillations in $(Bi_{1-x}Sb_x)_2Te_3Ag_y$ crystals were investigated at liquid helium temperature with the magnetic field vector was directed along the C_3 axis. For this orientation of the vector **B** the cross sections of all six ellipsoids of the upper valence band of the Fermi surface are the same. Oscillations of the transverse magnetoresistivity ρ_{xx} are shown in Fig. 3 for some $Sb_2Te_3Ag_y$ samples. A single oscillation frequency is observed in these crystals although the lower valence band is filled at this high hole concentration. The absence of oscillations from the lower valence band is attributable to the higher values of the effective mass in this band and is normal for Sb_2Te_3 (see, for example [4, 6]).

Shubnikov–de Haas oscillations in $(Bi_{1-x}Sb_x)_2Te_3Ag_y$ samples are shown in Fig. 4. For $Bi_{0.5}Sb_{1.5}Te_3Ag_{0.003}$ the Shubnikov–de Haas effect was also studied when the magnetic field vector **B** was rotated in the plane C_3C_1, see Fig. 5. The area of the extreme cross section S_H of the Fermi surface can be determined from the frequency of the Shubnikov–de Haas oscillations F: $S_H = 2\pi e[F/\hbar]$. Values of the oscillation frequency F are given in Tables 4 and 5.

We now turn our attention to the oscillations of the Hall resistivity ρ_{xy} as a function of the magnetic field (see Fig. 4). When the temperature falls below 4.2 K, these oscillations have the form of horizontal plateaus as in the quantum Hall effect. The oscillations typical exhibit phase singularities: the beginning of the downward deflection of $\rho_{xy}(B)$ corresponds to the resistivity minimum. These oscillations are caused by the existence of a lower valence band having a high density of states, which is filled in these samples, and by redistribution of holes between the upper [from which the oscillations of $\rho_{xx}(B)$ are observed] and the lower valence bands. This effect is discussed in further detail in [8].

4. DISCUSSION OF RESULTS

The first Brillouin zone of Sb_2Te_3 is similar to the Brillouin zone of an fcc lattice but is highly compressed along the z-axis. The energy spectrum of the Sb_2Te_3 crystal has two valence bands: a light hole band or upper valence band (UVB) and a heavy hole band or lower valence band (LVB), see Fig. 6. As can be seen from Fig. 6, there are also two conduction bands, an upper (UCB) and a lower (LCB) conduction band.

Table 4. $Sb_2Te_3Ag_y$

y	F, T	E_F, meV	p_{SdH}, 10^{19} cm^{-3}	$1/eR$, 10^{19} cm^{-3}
0	52.0	98	2.20	10.5
0.0035	76.5	144	5.64	22.3
0.0093	78.0	147	5.80	28.4
0.0100	115.0	217	10.40	52.1
0.0152	120.8	228	11.20	69.4

Table 5. $Bi_{0.5}Sb_{1.5}Te_3Ag_y$

y	F, T	E_F, meV	p_{SdH}, 10^{19} cm^{-3}	$1/eR$, 10^{19} cm^{-3}
0	56.8	100	3.28	6.9
0.0014	64.6	114	3.97	16.9
0.0030	82.6	146	5.76	20.2
0.0048	92.0	163	6.74	39.0

The Fermi surface of the upper valence band of Sb_2Te_3 is described by the six-ellipsoid Drabble–Wolfe model [9]. Both valence bands and the lower conduction band each have six Fermi-surface ellipsoids [5]. The six Fermi-surface ellipsoids are positioned as shown in Fig. 7a. One of the axes of the ellipsoid centered in the xz plane is parallel to the y (C_2)-axis. The major axes of the ellipsoids are inclined in the mirror plane $xz(C_1C_3)$ with respect to the crystallographic axes by the angle θ (Fig. 7b) which is determined as follows:

$$\tan 2\theta = 2\alpha_{23}/(\alpha_{22} - \alpha_{33}), \qquad (1)$$

where $\alpha_{ij} = m_0/m_j$ are the components of the tensor of the reciprocal effective masses which depend on energy

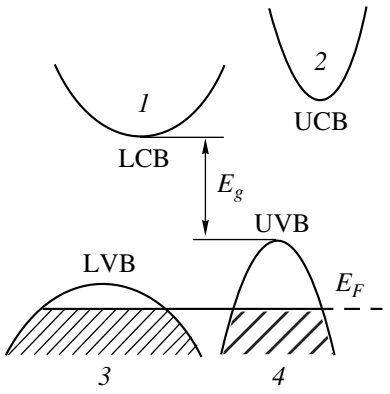

Fig. 6. Band structure of antimony telluride: (*1*, *2*) are the two extrema of the conduction band; (*3*, *4*) are the two extrema of the valence band, E_g is the indirect band gap, and E_F are the Fermi levels in p-type samples.

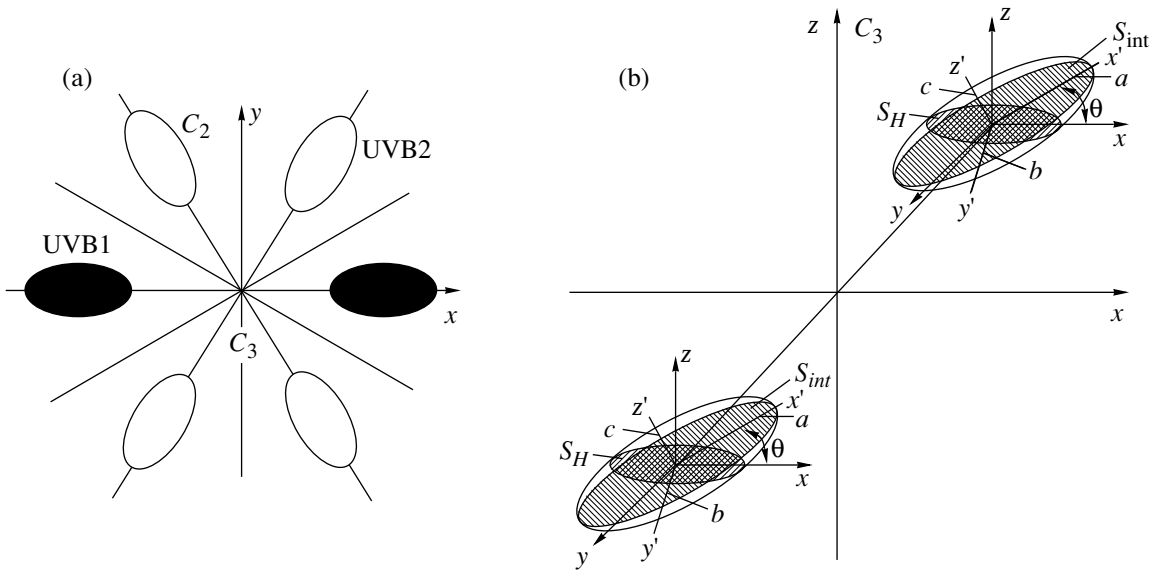

Fig. 7. Six-ellipsoid Fermi surface of the upper valence band of antimony telluride: (a) view in the *xy* plane perpendicular to the C_3-axis and (b) position of ellipsoids in the *xz* plane; C_2 is the twofold axis, θ is the angle of inclination of the ellipsoids to the basal plane, *x*', *y*', *z*' are the canonical coordinates of an ellipsoid having the semiaxes *a*, *b*, *c*.

because of some nonparabolicity of the spectrum. The angle θ in $(Bi_{1-x}Sb_x)_2Te_3$ crystals is only known as far as $x = 0.6$ [10] and is approximately 42° for $(Bi_{0.4}Sb_{0.6})_2Te_3$. For the mixed $Bi_{0.5}Sb_{1.5}Te_3$ crystals studied here the angle $\theta \approx 46°$ was determined by extrapolation.

In accordance with the ellipsoidal nonparabolic model, the general form of the Fermi surface in the upper valence band may be described by the following expression:

$$\alpha_{11}k_x^2 + \alpha_{22}k_y^2 + \alpha_{33}k_z^2 + \alpha_{23}k_yk_z = 2m_0E/\hbar^2, \quad (2)$$

where $k_{x,y,z}$ are the components of the wave vector, k_x is normal to the mirror plane in which the C_2- and C_3-axes lie, k_y is parallel to the C_2-axis, and k_z is parallel to the C_3-axis. In principle, the values of α_{ij} depend on energy but the Fermi surface remains ellipsoidal. It is interesting to study the dependence of the cross-sectional area S_H of each ellipsoid with its plane perpendicular to the direction of the magnetic field vector on the angle of inclination φ of this vector relative to the *z*-axis (C_3). In the experiments the direction of the field was varied in the *zx* (C_3C_1 plane). In this case, the six ellipsoids can be arbitrarily divided into two groups: two lying in this plane (UVB1) and the other four positioned outside this plane and being symmetric to it (UVB2) (Fig. 7a). By virtue of this symmetry, the ellipsoids in each group are equivalent in the sense that their cross-sectional areas S_H are the same for any φ. For a nonzero angle φ the cross sections of the ellipsoids in the same group differ from those of the ellipsoids in the other group. Thus, the ellipsoids in each group should be considered separately.

We introduce the following notation: *a*, *b*, and *c* are the principal axes of the ellipsoids; S_{min}, S_{max}, and S_{int} are the extreme cross sections of the ellipsoid. By S_H we denote the ellipsoid cross section with its plane passing through the center of the ellipsoid and perpendicular to the magnetic field vector, which is directed along the *z* (C_3)-axis in Fig. 7b. One of the axes of each of the two ellipsoids centered in the *xz* plane is parallel to the *y* (C_2) coordinate axis. The major axes of the ellipsoids are inclined in the C_1C_3 planes by the angle θ with respect to the crystallographic axes, which is determined by formula (1). The ellipsoid semiaxes may be expressed as:

$$a = \frac{1}{\hbar}\left(\frac{2m_0E_F}{\alpha'_{11}}\right)^{1/2}, \quad b = \frac{1}{\hbar}\left(\frac{2m_0E_F}{\alpha'_{22}}\right)^{1/2},$$
$$c = \frac{1}{\hbar}\left(\frac{2m_0E_F}{\alpha'_{33}}\right)^{1/2}, \quad (3)$$

where

$$\alpha'_{22} + \alpha'_{33} = \alpha_{22} + \alpha_{33},$$
$$\alpha'_{22}\alpha'_{33} = \alpha_{22}\alpha_{33} - (\alpha_{23})^2. \quad (4)$$

Using simple transformations, we obtain expressions for the extreme cross sections of the ellipsoid:

$$S_{\min} = \pi cb = \frac{2m_0E_F}{(\alpha'_{22}\alpha'_{33})^{1/2}\hbar^2},$$

$$S_{\max} = \pi ac = \frac{2m_0E_F}{(\alpha'_{11}\alpha'_{33})^{1/2}\hbar^2}, \quad (5)$$

$$S_{\text{int}} = \pi ab = \frac{2m_0E_F}{(\alpha'_{11}\alpha'_{22})^{1/2}\hbar^2}.$$

Simple transformations then yield the following dependence of the extreme cross sections of the Fermi surface for the two UVB1 ellipsoids:

$$S_{H1} = 2\pi m_0E_F/\hbar^2(\alpha'_{22}\alpha'_{33}\sin^2\theta + \alpha'_{11}\alpha'_{22}\cos^2\theta)^{1/2}, \quad (6)$$

where φ is the experimental value of the angle between the direction of the magnetic field vector and the *z* axis, and θ is the angle of inclination of the ellipsoid axes with respect to the crystallographic axes.

For the four UVB2 ellipsoids we obtain

$$S_{H2} = 4\pi m_0E_F/\hbar^2$$
$$\times [4(\alpha'_{22}\alpha'_{33}\sin^2\theta + \alpha'_{11}\alpha'_{22}\cos^2\theta)\cos^2\varphi$$
$$+ (\alpha'_{11}\alpha'_{22}\sin^2\theta + 3\alpha'_{11}\alpha'_{33} + \alpha'_{22}\alpha'_{33}\cos^2\theta)\sin^2\varphi \quad (7)$$
$$+ \alpha'_{22}(\alpha'_{11} - \alpha'_{33})\sin 2\theta \sin 2\varphi]^{1/2}.$$

The hole concentration in the six ellipsoids is given by

$$p = \frac{6 \times 2V}{(2\pi\hbar)^3}, \quad (8)$$

where the volume of a single ellipsoid is $V = 4\pi abc/3$.

Using the data obtained from a study of the Shubnikov–de Haas effect in $(Bi_{1-x}Sb_x)_2Te_3Ag_y$ crystals, we calculated the hole concentrations in the upper valence band for the six-ellipsoid Fermi surface and the Fermi energy and the results are given in Tables 4 and 5. We used the following band parameters: $\alpha'_{11} = 2.26$, $\alpha'_{22} = 32.5$, and $\alpha'_{33} = 11.6$ [6].

Figure 8 gives theoretical (curves) and experimental (symbols) dependences of the areas of the extreme cross sections of the Fermi-surface ellipsoids on the angle of inclination of the magnetic field vector relative to the C_3-axis in the C_1C_3 plane for UVB1 and UVB2 ellipsoids. The solid curves give the theoretical angular dependences of the cross-sectional areas of ellipsoids for which the anisotropy of the extreme cross sections is $S_{\max}/S_{\min} = 3.8$. It can be seen that for this anisotropy the experimental points are a good fit to the theoretical curves. Also plotted are similar curves for ellipsoids with different band parameters. The dotted curves refer to ellipsoids with 1.4 times lower anisotropy ($S_{\max}/S_{\min} = 2.8$) and the dot-dash curves refer to ellipsoids having anisotropy 1.4 times higher than 3.8 ($S_{\max}/S_{\min} = 5.4$). It can be seen that these curves differ from the experimental points (the size of the point approximately corresponds to the error in determining the extreme cross section of the Fermi surface) from which it follows that values of $S_{\max}/S_{\min} \approx 3.8$ may be considered suitable for samples of this particular composition.

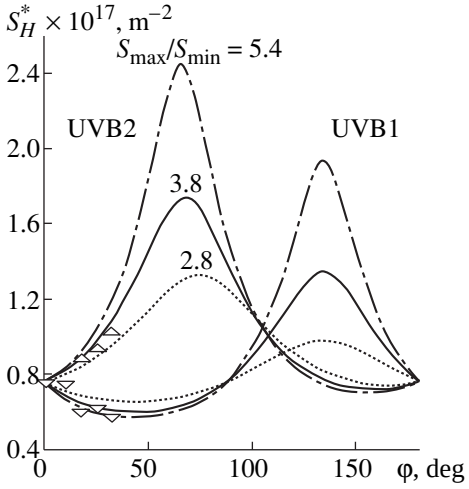

Fig. 8. Theoretical (curves) and experimental (symbols) dependences of the areas of the extreme surface cross sections S_H on the angle φ between the C_3 crystal axis and the vector **B** when the magnetic field is rotated in the C_1C_3 plane. The theoretical dependences are plotted for various values of the anisotropy $S_{\max}/S_{\min}$ of the Fermi surface (indicated in the figure).

The hole concentrations p_{SdH} in the upper valence band calculated using the Shubnikov–de Haas effect were compared with the corresponding Hall concentrations $1/eR$. All these values are given in Tables 4 and 5 which show that the values of p_{SdH} are always lower than the corresponding values of $1/eR$, confirming that the second lower valence band (LVB) is filled at these high hole concentrations.

Thus, a study of the resistivity, Hall effect at different temperatures, and Shubnikov–de Haas effect in $(Bi_{1-x}Sb_x)_2Te_3Ag_y$ single crystals has shown that unlike Bi_2Te_3, in Sb_2Te_3 and $Bi_{0.5}Sb_{1.5}Te_3$ crystals silver exhibits acceptor properties: the hole concentration increases with increasing silver content in the crystal.

An investigation of the angular and concentration dependences of the Shubnikov–de Haas effect with silver doping showed that the anisotropy of the upper valence band ellipsoids for $(Bi_{1-x}Sb_x)_2Te_3Ag_y$ remains the same as $(Bi_{1-x}Sb_x)_2Te_3$.

REFERENCES

1. B. M. Gol'tsman, V. A. Kudinov, and I. A. Smirnov, *Semiconducting Thermoelectric Materials Based on Bi_2Te_3* (Nauka, Moscow, 1972).

2. J. Horak, P. Lostak, and L. Benes, Philos. Mag. B **50**, 665 (1984).
3. P. Lostak, J. Horak, and L. Koudelka, Phys. Status Solidi A **76**, K71 (1983).
4. V. A. Kulbachinskiĭ, Z. M. Dashevskiĭ, M. Inoue, *et al.*, Phys. Rev. B **52**, 10915 (1995).
5. V. A. Kulbachinskiĭ, N. Miura, H. Arimoto, *et al.*, J. Phys. Soc. Jpn. **68**, 3328 (1999).
6. V. A. Kulbachinskiĭ, N. Miura, H. Nakagawa, *et al.*, J. Phys.: Condens. Matter **11**, 5273 (1999).
7. J. Navratil, I. Klichova, S. Karamazov, *et al.*, J. Solid State Chem. **140**, 29 (1998).
8. V. A. Kul'bachinskiĭ, A. Yu. Kaminskiĭ, N. Miyajima, *et al.*, Pis'ma Zh. Éksp. Teor. Fiz. **70**, 754 (1999) [JETP Lett. **70**, 767 (1999)].
9. J. R. Drabble and R. Wolfe, Proc. Phys. Soc. London, Sect. B **69**, 1101 (1956).
10. H. Kohler and A. Freudenberger, Phys. Status Solidi B **84**, 195 (1977).

Translation was provided by AIP